



Article

Monitoring the Invasive Plant *Spartina alterniflora* in Jiangsu Coastal Wetland Using MRCNN and Long-Time Series Landsat Data

Wenqing Zhu ¹, Guangbo Ren ², Jianping Wang ³, Jianbu Wang ^{2,*}, Yabin Hu ², Zhaoyang Lin ⁴, Wei Li ⁴, Yajie Zhao ⁵, Shibao Li ¹ and Ning Wang ³

- ¹ College of Oceanography and Space Informatics, China University of Petroleum (East China), Qingdao 266580, China; z20160045@s.upc.edu.cn (W.Z.); lishibao@upc.edu.cn (S.L.)
- ² Lab of Marine Physics and Remote Sensing, First Institute of Oceanography, Ministry of Natural Resources, Qingdao 266061, China; renguangbo@fio.org.cn (G.R.); huyabin@fio.org.cn (Y.H.)
- ³ Shandong Provincial Key Laboratory of Restoration for Marine Ecology, Shandong Marine Resources and Environment Research Institute, Yantai 264006, China; wangjianping01@shandong.cn (J.W.); 18905455956@189.cn (N.W.)
- ⁴ School of Information and Electronics, Beijing Institute of Technology, Beijing 100081, China; 3120190780@bit.edu.cn (Z.L.); liw@bit.edu.cn (W.L.)
- ⁵ Department of Science Research, Shandong Yellow River Delta National Nature Reserve Administration, Dongying 257091, China; hhsjzstjczx@dy.shandong.cn
- * Correspondence: wangjianbu@fio.org.cn



Citation: Zhu, W.; Ren, G.; Wang, J.; Wang, J.; Hu, Y.; Lin, Z.; Li, W.; Zhao, Y.; Li, S.; Wang, N. Monitoring the Invasive Plant *Spartina alterniflora* in Jiangsu Coastal Wetland Using MRCNN and Long-Time Series Landsat Data. *Remote Sens.* **2022**, *14*, 2630. <https://doi.org/10.3390/rs14112630>

Academic Editor: Nereida Rodriguez-Alvarez

Received: 25 April 2022

Accepted: 28 May 2022

Published: 31 May 2022

Publisher's Note: MDPI stays neutral with regard to jurisdictional claims in published maps and institutional affiliations.



Copyright: © 2022 by the authors. Licensee MDPI, Basel, Switzerland. This article is an open access article distributed under the terms and conditions of the Creative Commons Attribution (CC BY) license (<https://creativecommons.org/licenses/by/4.0/>).

Abstract: Jiangsu coastal wetland has the largest area of the invasive plant, *Spartina alterniflora* (*S. alterniflora*), in China. *S. alterniflora* has been present in the wetland for nearly 40 years and poses a substantial threat to the safety of coastal wetland ecosystems. There is an urgent need to control the distribution of *S. alterniflora*. The biological characteristics of the invasion process of *S. alterniflora* contribute to its multi-scale distribution. However, the current classification methods do not deal successfully with multi-scale problems, and it is also difficult to perform high-precision land cover classification on multi-temporal remote sensing images. In this study, based on Landsat data from 1990 to 2020, a new deep learning multi-scale residual convolutional neural network (MRCNN) model was developed to identify *S. alterniflora*. In this method, features at different scales are extracted and concatenated to obtain multi-scale information, and residual connections are introduced to ensure gradient propagation. A multi-year data unified training method was adopted to improve the temporal scalability of the MRCNN. The MRCNN model was able to identify the annual *S. alterniflora* distribution more accurately, overcame the disadvantage that traditional CNNs can only extract feature information at a single scale, and offered significant advantages in spatial characterization. A thematic map of *S. alterniflora* distribution was obtained. Since it was introduced in 1982, the distribution of *S. alterniflora* has expanded to approximately 17,400 ha. In Jiangsu, the expansion process of *S. alterniflora* over time was divided into three stages: the growth period (1982–1994), the outbreak period (1995–2004), and the plateau period (2005–2020). The spatial expansion direction was mainly parallel and perpendicular to the coastline. The hydrodynamic conditions and tidal flat environment on the coast of Jiangsu Province are suitable for the growth of *S. alterniflora*. Reclamation of tidal flats is the main factor affecting the expansion of *S. alterniflora*.

Keywords: *Spartina alterniflora*; Jiangsu; time series Landsat images; deep learning; MRCNN; tidal flat reclamation

1. Introduction

Spartina alterniflora (*S. alterniflora*), which is a perennial herb, is native to the Atlantic coast of North America and inhabits tidal environments, such as estuaries and bays [1]. With its robust adaptability and reproductive ability, it quickly takes root and spreads in a

suitable environment and can become the dominant species in salt marsh wetlands [2,3]. *S. alterniflora* was introduced to the coast of Jiangsu Province in China in approximately 1982, and it has played a substantial role in promoting the deposition of silt to form new land [4]. *S. alterniflora* salt marsh has become the main target of reclamation on the Jiangsu tidal flat. However, according to recent studies [5–7], *S. alterniflora* poses an important ecological threat to the coastal environment of Jiangsu, replacing native species, changing the foraging environment for birds, blocking tidal flows and rivers, and reducing biodiversity. Tidal flat reclamation has an important influence on the growth of *S. alterniflora* and the stability of ecosystems [8]. Reclamation can change the hydrodynamic environment of tidal flats [9] and affect the distribution of *S. alterniflora* [10]. At present, the scientific management of *S. alterniflora* along the coast of Jiangsu requires sufficient quantitative monitoring data to deal effectively with the ecological consequences of the invasion and expansion of *S. alterniflora*. A long time series of monitoring data over a large area is essential for the ecological protection and development of coastal wetlands.

Compared with traditional field surveys, remote sensing technology has the advantages of large area monitoring and long time series data. It can obtain information about the temporal and spatial distribution of *S. alterniflora* effectively and accurately [11,12]. Remote sensing has always been considered one of the most effective tools for monitoring invasive plants [13]. Generally, satellite imagery with medium spatial resolution, such as Landsat data, is suitable for monitoring the distribution of *S. alterniflora* over a large area [11,12,14]. The Landsat program is by far the longest earth monitoring satellite project, and its series of satellites have intensive image acquisition capabilities, which make it easier to obtain high-quality images [15]. The availability of remote sensing data and the development of computer information technology provide a reliable choice for large-area continuous monitoring of *S. alterniflora*. However, the classification accuracy of coastal wetland ecosystems with complex land cover patterns needs to be further improved [16]. Most of the classification methods used to date are traditional machine learning algorithms, such as maximum likelihood, support vector machine, and random forest [17–19]. Some researchers have also classified *S. alterniflora* using training decision rules [20,21]. These methods have limited ability to deal with complex function models, and their level of automation is low, which makes it difficult to improve the classification accuracy in complex coastal wetland scenes. Therefore, extracting information on *S. alterniflora* from a large area and long time series remote sensing data is still a challenging task that requires the development of more powerful classification methods.

Deep learning, which essentially transforms the underlying attributes of the original data into more robust abstract features by learning multi-layer nonlinear network structures and realizes a powerful ability to learn the essential features of data from the sample, is a new field in machine learning [22]. Using a convolutional neural network (CNN) to automatically extract features from remote sensing data has greatly improved the classification accuracy of ground objects in complex environments [23–25]. In deep learning, CNN is the dominant supervised learning algorithm for classification because it has proved to be superior to the traditional machine learning classification methods [26]. The use of CNN has made a series of breakthroughs in many remote sensing applications, including classification, semantic segmentation, and object detection [27–29]. In recent years, deep learning has been widely used in wetland vegetation classification. For example, Guo et al. used a mangrove extraction network (ME-Net) to classify mangroves on Hainan Island, with an overall accuracy of 97.48% for mangrove extraction [30]; Hosseiny et al. used the Sentinel dataset and the WetNet model to classify complex wetland areas in Newfoundland, Canada. The experiments showed that WetNet was superior to other comparative models in classification accuracy and processing time [31]; Mohammadimanesh et al. also proved the effectiveness of residual units in the classification of coastal wetland vegetation [32]. However, relatively little research is focused on the identification of *S. alterniflora* distribution in long time series data using deep learning. At present, the research mainly focuses

on identification from small-area or mono-temporal image data [33,34] and the analysis of spectral phenological characteristics of *S. alterniflora* [35].

The geographical features of China's coastal zone are complicated and diverse. *S. alterniflora* shows different invasion abilities in different areas, and the competitive relationship between *S. alterniflora* and local vegetation also varies. The coastal zone of Jiangsu has distinct geographical features, with a straight muddy coast from north to south, and it has the largest tidal flat area in China. In Jiangsu Province, *S. alterniflora* has invaded and expanded for nearly 40 years, and it has the largest distribution area in China. *S. alterniflora* appears at various states and scales during the invasion process, such as small discrete patches at the early stage of invasion; connected strips, large broken patches, and mixed patches at the mid-invasion stage; and large monoculture patches at the end of the invasion stage. These different states exist at the same time in any intrusion area. For the identification of ground objects such as *S. alterniflora* with complex growth states, the classical CNN model causes the gradient to disappear as the number of layers increases. Therefore, in the current study, the MRCNN model and post-processing method were proposed to obtain multi-temporal identification of *S. alterniflora*. An MRCNN combines the advantages of the Inception [36,37] and ResNet [38,39] CNN models. First, the MRCNN extracts features on different scales and obtains rich multi-scale information [40], and second, the residual structure is used to directly connect the shallow and deep layers, and the larger gradient is directly propagated to the deeper layer, which reduces the computational complexity. Using long time series remote sensing data for the large coastal wetland area in Jiangsu, this study proposed a deep learning MRCNN model suitable for the identification of *S. alterniflora* in Jiangsu to expand the application potential of deep learning. A unified training method for multi-temporal Landsat data was also adopted to improve the temporal scalability of the deep learning model. Field survey data, Landsat data, and the classification method proposed in this study were used to identify *S. alterniflora* in a complex coastal wetland environment and a thematic map of *S. alterniflora* distribution in Jiangsu Province from 1990 to 2020 was created. Finally, this study analyzed the influencing factors and the temporal and spatial rules of *S. alterniflora* expansion to provide reliable data and technical support for remote sensing monitoring and scientific management of *S. alterniflora* in Jiangsu Province.

2. Materials

2.1. Study Area

The study area is located along the coast of Jiangsu Province, China (between 119°21'E and 121°55'E, 31°33'N and 35°07'N) (as shown in Figure 1). The coastline of Jiangsu Province has a total length of 954 km. It stretches from the Xiuzhen estuary in the north to the estuary of the Yangtze River in the south and faces the Yellow Sea in the east. There are three cities in the coastal zone of Jiangsu, namely Lianyungang, Yancheng, and Nantong. Controlled by the monsoon climate, the coastal zone of Jiangsu is located in the transition zone between the north subtropical zone and the warm temperate zone and is influenced by both maritime and continental climates. The average annual temperature is 14 °C, and the average annual rainfall is 1000 mm [41]. The average tidal range along the coast of Jiangsu is 1–4 m. Many rivers enter the sea in this region, and the tidal salinity is low. There is a large muddy tidal flat, and the upper part of the intertidal zone suitable for the growth of *S. alterniflora* can be up to 4 km wide [42]. Both the climate and the tidal flat sediment provide suitable conditions for the growth and expansion of *S. alterniflora* [43]. More than 90% of the coastal areas in Jiangsu are muddy, and Jiangsu currently has the largest area of tidal flats in China [44]. The Red-Crowned Crane National Nature Reserve (RCCNNR) and the Elk National Nature Reserve (ENNR) are both located in Yancheng, central Jiangsu Province. The wetland vegetation in the reserves mainly includes *S. alterniflora* at the forefront of the tidal flat, *Phragmites australis* in freshwater areas, and *Suaeda* in the high intertidal zone [45]. Yancheng has become the largest area of *S. alterniflora* in China [46].



Figure 1. Coastline of the three major cities in Jiangsu Province: Lianyungang, Yancheng, and Nantong. The red triangles are the site of field investigation. The green areas are the Yancheng National Nature Reserve.

Owing to policy changes, the coastline of Jiangsu Province has been greatly disturbed by human activities. Since 1996, a strategy of Marine Sudong, which is characterized by large area development, has been implemented in the Yancheng coastal wetland, accelerating the pace of reclamation. Large areas of coastal wetlands have been used to build artificial aquaculture ponds. In 2019, the Yancheng Nature Reserve was listed as a World Natural Heritage Site, which restricts and regulates further human activities [45].

2.2. Data and Pre-Processing

Jiangsu Province introduced *S. alterniflora* in many areas in 1982 [4]. In the incubation period of early introduction (1982–1986), *S. alterniflora* cannot be identified in Landsat images with a spatial resolution of 30 m. Therefore, this study obtained a total of 21 original Landsat images for seven time periods at 5-year intervals: 1990, 1995, 2000, 2005, 2010, 2015, and 2020 (as shown in Table 1). The collected images were cloud-free in the study area. The time of the image data is very important for accurately distinguishing *S. alterniflora* from other salt marsh plants. On the basis of the local phenological characteristics of *S. alterniflora*, the selected remote sensing images were concentrated in August–October, when *S. alterniflora* was in its most vigorous growth period [47,48], and its spectral features were well differentiated from indigenous vegetation. However, because of the large study area and the need to avoid cloud-cover in the images, it was difficult to obtain images that completely covered the study area and met the monthly conditions within a single year. Therefore, missing images were taken from adjacent years to minimize the data loss caused

by cloud cover. In this paper, a series of pre-processing of Landsat data was performed using ENVI 5.3 software. The digital numbers were converted to radiance by radiometric calibration. The atmospheric correction method used was Quick Atmospheric Correction (QUAC). Finally, band combination, image mosaicking, and clipping were performed. Because the data came from different sensors with different spatial resolutions, to unify the data to a spatial resolution of 30 m, this study did not fuse the panchromatic and multispectral bands in Landsat 8 OLI data. The reason was that compared with Landsat 8 OLI, Landsat 5 TM lacked a panchromatic band with a spatial resolution of 15 m. A total of six original bands of Red, Green, Blue, NIR, SWIR-1, and SWIR-2 were selected. The wavelength ranges of NIR, SWIR-1, and SWIR-2 of Landsat 5 TM were 0.760–0.900, 1.550–1.750, 2.080–2.350, respectively. The wavelength ranges of NIR, SWIR-1, and SWIR-2 of Landsat 8 OLI were 0.845–0.885, 1.560–1.660, and 2.100–2.300.

Table 1. Overview of Landsat data after band combination used in this study. (Date format: month/day/year).

Period	Sensor	Imaging Time	Resolution (m)	Number of Bands
1990	Landsat 5 TM	10/21/1989 10/30/1989 10/31/1990	30	6
1995	Landsat 5 TM	08/03/1995 08/12/1995 09/27/1995	30	6
2000	Landsat 5 TM	08/21/2000 09/17/2000 10/10/2000	30	6
2005	Landsat 5 TM	08/20/2004 10/08/2005 10/17/2005	30	6
2010	Landsat 5 TM	09/19/2009 10/03/2009 10/31/2010	30	6
2015	Landsat 8 OLI	08/03/2015 09/18/2015 10/13/2015	30	6
2020	Landsat 8 OLI	10/31/2019 08/16/2020 09/08/2020	30	6

2.3. Field Investigation

A field investigation of *S. alterniflora* in the coastal wetlands of Jiangsu Province was conducted in October 2020, collecting data from 54 survey sites, 52 drone flights, and hundreds of photographs (as shown in Figure 2). The survey sites were concentrated in Yancheng because Yancheng is a typical distribution area of *S. alterniflora* in the coastal wetlands of Jiangsu Province. The site distribution is shown in Figure 1. The photographs taken by the drone reflect the distribution characteristics of *S. alterniflora* at various scales in the coastal wetlands of Jiangsu Province. On the basis of the drone photographs, the spectral characteristics, and growth characteristics of *S. alterniflora*, this study obtained a ground truth map of *S. alterniflora* in Jiangsu Province using ArcGIS 10.2 software. This map was used as the label image of the deep learning model. Figure 3 illustrates the spectral characteristics of *S. alterniflora* and several other ground feature types. It can be seen that the types were well distinguished in the wavelength range of the NIR band.

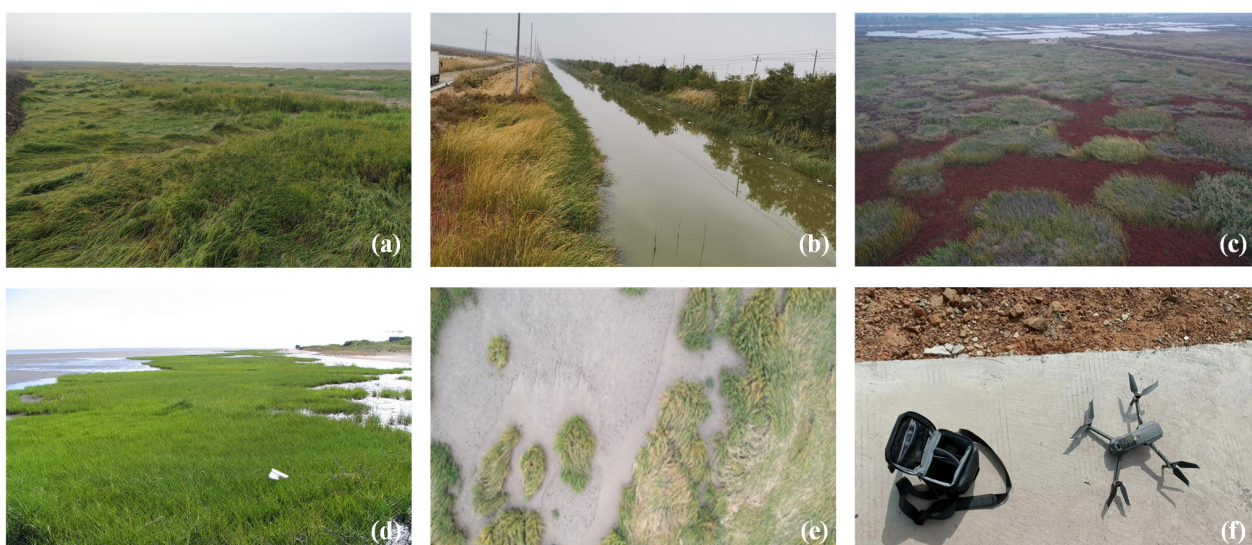


Figure 2. Field survey photographs. (a) *Spartina alterniflora* in a saturated ecological niche; (b) *S. alterniflora* on both sides of the tidal creek; (c) *S. alterniflora* mixed with *Suaeda*. *Suaeda* is reddish-brown and *S. alterniflora* is green; (d) *S. alterniflora* at the forefront of the tidal flat; (e) *S. alterniflora* photographed by drone at an altitude of 30 m; (f) drones used to acquire field data. The drone model is DJI Mavic 2.

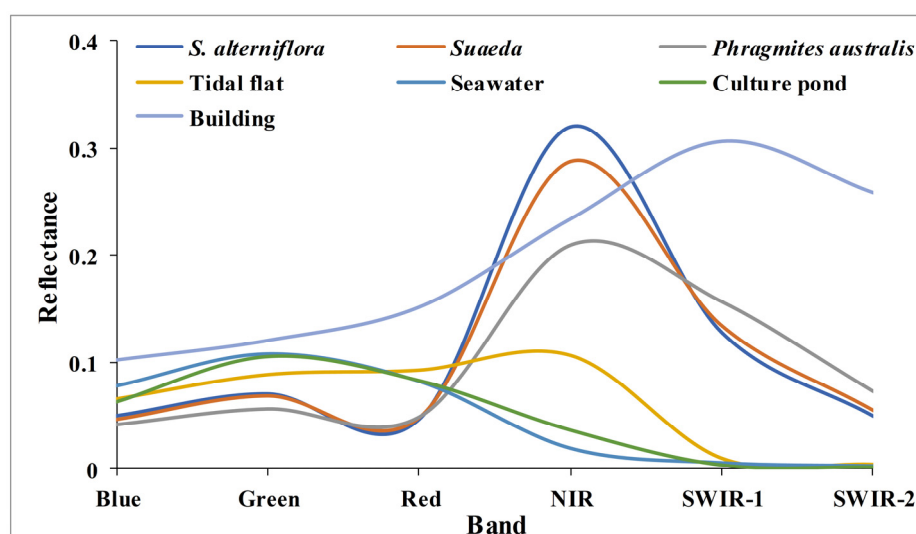


Figure 3. Spectral curves of the seven typical classes in the study area (from the Landsat 8 OLI image acquired on 16 August 2020).

3. Methods

3.1. MRCNN Structure

At present, the main multispectral pixel-level classification methods include support vector machine (SVM), random forest (RF), and neural networks. A convolutional neural network (CNN) is a feedforward neural network that uses convolutional operations and has a deep structure. According to literature and experiments [27–29], CNNs are widely used owing to their excellent performance. Thus, a CNN was employed for experimentation and prediction, as shown below.

The performance of the visual geometry group network does not always improve as the number of layers increases, mainly because of the vanishing gradients in classical CNNs. To reduce the computational cost and ensure that the gradient was propagated in deeper layers, we proposed two representative networks: Inception V1 and ResNet. Inception V1

performs feature extraction and pooling at different scales to obtain information at multiple scales and then superimposes the features for output. Inception V1 can greatly reduce the number of calculations needed to ensure the propagation of gradients, which is its most important advantage [36,37]. ResNet uses residual connections to propagate gradients, that is, the shallower layers are directly connected with the deeper layers. Directly propagating larger gradients into deeper layers is both understandable and efficient [38,39]. The focus of this study was the temporal and spatial distribution of *S. alterniflora* in Jiangsu Province over the past 30 years. *S. alterniflora* has been found at different scales, such as small discrete patches, connected strips, large broken patches, and mixed patches from the growth period to the outbreak period and then to the plateau period. Inspired by CD-CNN, Inception V1, and ResNet, a multi-scale residual convolutional neural network (MRCNN) was proposed. The structure is shown in Figure 4. It has the characteristics of deep residual network skip-layer identity mapping and also overcomes the disadvantage that traditional CNNs can only extract feature information at a single scale.

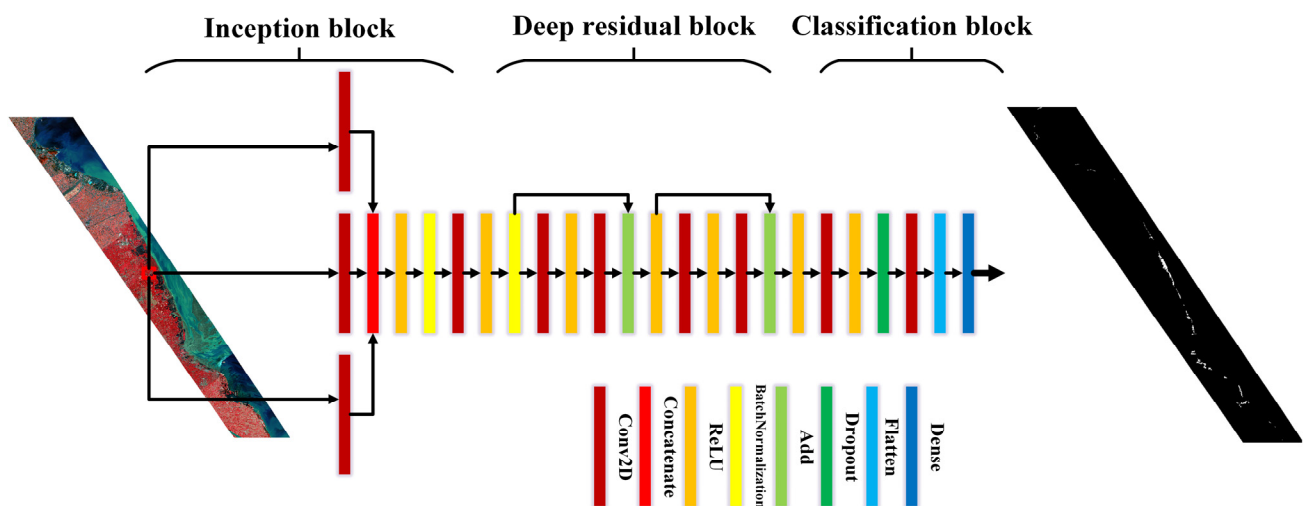


Figure 4. Overall construction of proposed multi-scale residual convolutional neural network (MRCNN).

The MRCNN was divided into three blocks: the inception block, deep residual block, and classification block. The main structure of the inception block used three convolutional layers with different convolution kernels to simultaneously extract the features of the samples. The sizes of convolution kernels set in this study were 1×1 , 3×3 , and 5×5 , respectively. Then, the extracted features of each convolution layer were concatenated. The main role of the inception block was to extract multi-scale features and reduce computational complexity. In this study, a batch normalization layer was applied between the convolution layer and the rectified linear unit (ReLU) activation layer to reduce the drift of the internal covariance and accelerate the convergence of the network. The batch normalization layer normalizes the features to a fixed distribution. The specific operations are:

$$\hat{x}_i = \frac{x_i - \mu}{\sqrt{\sigma^2 + \varepsilon}} \quad (1)$$

$$y_i = \gamma \hat{x}_i + \beta \quad (2)$$

where \hat{x}_i and y_i are the input and output features of the i th kernel, respectively; the parameters γ and β represent the scale displacement; ε is a constant close to 0.

The depth residual block was then used to directly connect the features of the shallow layers to the deep layers to ensure gradient propagation. During the forward propagation of the algorithm, a skip connection is formed between convolutional layers to realize the identity mapping of input and output. The structure of the convolution layer + ReLU

activation function + convolution layer was used to better extract features and suppress gradient loss. Each convolution kernel was set to 1×1 to reduce computational complexity and save time. Assuming that x represents input and $F(x)$ represents residual mapping, the output of the residual unit is:

$$H(x) = F(x) + x \quad (3)$$

When the residual $F(x) = 0$, the function of the residual unit is identity mapping. The output of layer L is:

$$H(x_L) = \sum_{i=1}^{L-1} F(x_i) + x_L \quad (4)$$

The inverse gradient is:

$$\frac{\partial loss}{\partial x_l} = \frac{\partial loss}{\partial H(x_L)} \quad (5)$$

where $\frac{\partial loss}{\partial x_l}$ is the gradient descent of the loss function.

In the final classification block, we added a dropout layer to enhance the generalization of the model. During the training process, the network randomly discards some neurons, which destroys the close interaction between features so that the network does not rely on local features too much. In this block, all three-dimensional features were flattened into one-dimensional features for subsequent classification. The classification block used a fully connected layer to map features to class numbers and then used the Softmax activation function and cross-entropy loss function. The Softmax function is defined as:

$$f(x_i) = \frac{e^{x_i}}{\sum_{i=1}^N e^{x_i}} \quad (6)$$

where the input and output of the Softmax function are x_i and $f(x_i)$, respectively, N is the number of categories, and $f(x_i)$ is the probability value predicted to be class i . The activation function helps with the pixel-level classification of *S. alterniflora* and background data.

3.2. Unified Training Method Based on MRCNN

The accuracy and applicability of the dataset directly determine the classification effect of the model. Because the distribution area of *S. alterniflora* in Jiangsu Province was relatively small in 1990, and the sample distribution was extremely unbalanced, the current study began to create a data set from the data in 1995. To improve the temporal scalability of the deep learning model, the method of training data adopted a unified training of the multiphase data approach instead of training a model for the data of each phase separately.

A random sliding window clipping method was used to obtain small sample blocks with a size of 9×9 . The 54 field survey sites in 2020 were selected as the sample selection areas for *S. alterniflora*. Samples were randomly selected in 1995, 2000, 2005, 2010, 2015, and 2020 from locations that covered 60% of the area of *S. alterniflora*. The number of background samples was 10 times that of the corresponding *S. alterniflora* samples every year. Figure 5 shows the spatial distribution of training samples in 2020 as an example. To capture the spatial characteristics of *S. alterniflora* better, a six-year sample was used as the training dataset. The diversity and variability of training data sets were increased through data standardization and data expansion [49]. Table 2 shows the training sets from 1995 to 2020. In this six-year period, we selected a total of 7131 *S. alterniflora* samples and 71,310 background samples, giving a total of 78,441 samples. Eighty percent of the samples in the training set were used for model training, and 20% of the samples were used for model validation. All the remaining data in the coastal areas of Jiangsu Province were used to test the model, and the identification and evaluation of *S. alterniflora* in each year were examined. The number of test samples from 1995 to 2020 is 312,527, 303,222, 301,792, 301,044, 300,791, and 300,384 respectively. In this process, different spatially and geographically independent samples were acquired for training and testing to prevent information from leaking from

the test dataset to the model. This ensured that the classification algorithm had good generalization ability, which was beneficial for analyzing the temporal and spatial change in *S. alterniflora*. Table 3 shows the composition of test samples per year, and the ratio of the number of model training samples to the number of test samples per year is about 1:3.8.

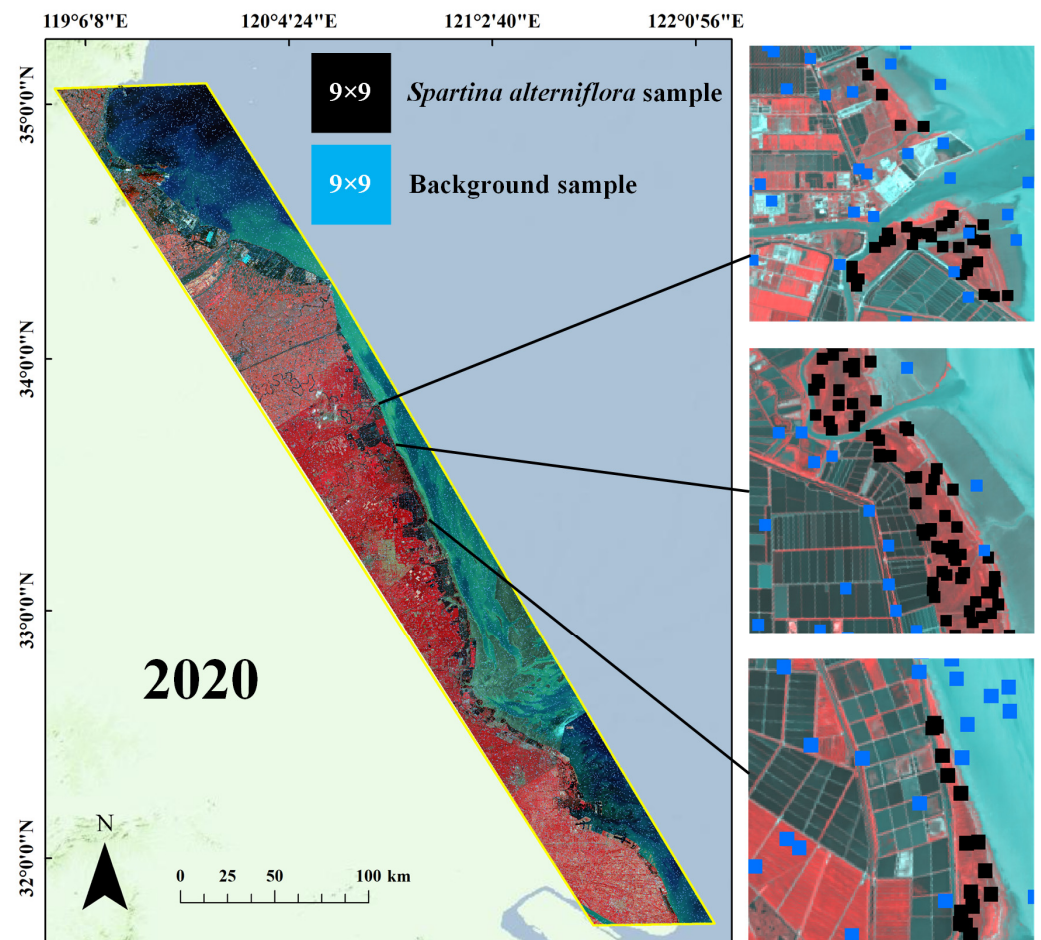


Figure 5. Spatial distribution of training samples in coastal Jiangsu in 2020. The number of samples is 15,983. The three pictures on the right are the enlarged details of the spatial distribution of the samples. The yellow box shows the coverage of the data in 2020.

Table 2. Distribution of training samples of MRCNN model.

Period	Number of <i>S. alterniflora</i> Samples	Number of Background Samples	Total
1995	349	3490	3839
2000	1195	11,950	13,145
2005	1325	13,250	14,575
2010	1393	13,930	15,323
2015	1416	14,160	15,576
2020	1453	14,530	15,983
Total	7131	71,310	78,441

Table 3. Distribution of test samples from 1995 to 2020.

Period	Number of <i>S. alterniflora</i> Samples	Number of Background Samples	Total
1995	233	312,294	312,527
2000	797	302,425	303,222
2005	884	300,908	301,792
2010	929	300,115	301,044
2015	945	299,846	300,791
2020	969	299,415	300,384

The research area of the current study was the coastal wetland on the Jiangsu coastline, and the study aimed to explore changes in the distribution of *S. alterniflora* in the coastal wetland. Considering the broad coverage of the data used in this study, there were more than 2.5×10^7 pixels per year. At the same time, in the test data, the number of *S. alterniflora* samples differed greatly from the number of background samples, which might have resulted in serious background misclassification in binary classification. To avoid this, the output results of the MRCNN were post-processed in this paper using ArcGIS 10.2 software. According to the complex growth characteristics and environment of *S. alterniflora*, the classification results were optimized using artificial coastline information. In this study, only the classification results on the seaward side were retained, and the classification results on the landward side were discarded. This helped guarantee the accuracy of the global classification results. The output of the MRCNN was a binary image representing *S. alterniflora* and the background. The whole process flow is shown in Figure 6. The final distribution map of *S. alterniflora* in each period was obtained by performing morphological processing such as dilation, erosion, and noise elimination on the post-processing results by MatlabR2020a software.

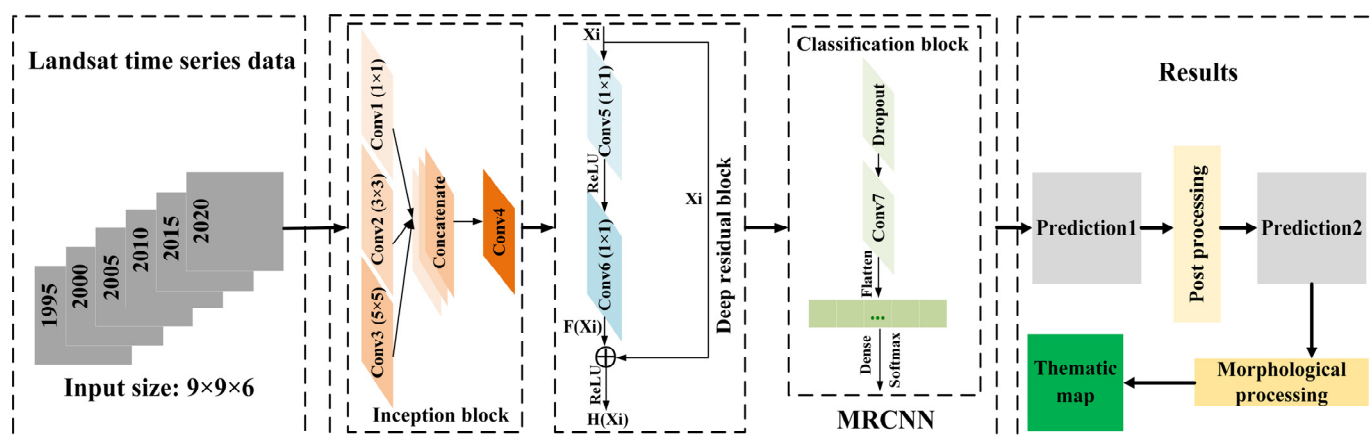


Figure 6. Unified training method based on MRCNN. The **left** part shows the input multi-temporal dataset, the **middle** part shows the three main blocks of MRCNN, and the **right** part shows the post-processing and morphological processing of the classification results to obtain the thematic map of *S. alterniflora* distribution.

In this set of experiments, accuracy, recall, precision, and F1-score were used as metrics. *S. alterniflora* was regarded as the positive class, and the others, such as vegetation, tidal flat, buildings, and water bodies, as the negative classes. The pixel value of *S. alterniflora* in the global truth map was set to 1, and the other pixel values were set to 0. Accuracy is the ratio of the number of correctly predicted samples to the total number of samples, and precision is the ratio of the number of correctly predicted positive samples to the total predicted positive samples. Recall is the ratio of the number of samples that are correctly predicted to be positive to the total number of samples that are actually positive, while

the F1-score is a quantitative indicator for data with an unbalanced sample distribution, which measures the balance between accuracy and recall rate. Accordingly, the F1-score is formulated as follows:

$$F - 1score = 2 \times \frac{\text{Precision} \times \text{Recall}}{\text{Precision} + \text{Recall}} \quad (7)$$

where precision and recall are obtained from:

$$\text{Precision} = \frac{\text{True positives}}{\text{True positives} + \text{False positives}} \quad (8)$$

$$\text{Recall} = \frac{\text{True positives}}{\text{True positives} + \text{False negatives}} \quad (9)$$

4. Results and Analysis

4.1. Testing of the Model

To better identify the advantages of the proposed MRCNN, a set of comparative experiments between CNNs were conducted. The selected comparison algorithms were CascadeNet and dual-tunnel CNN. CascadeNet [50] is a simple and efficient residual network. The dual-tunnel CNN [51] is a network specially designed for hyperspectral images and multispectral images. It contains a branch dedicated to extracting spatial information and a branch dedicated to extracting spectral information. These two CNNs are proven algorithms for efficient multispectral classification and are more than sufficient as comparison algorithms. The deep learning experiments were performed on a computer equipped with NVIDIA RTX2070S discrete graphics, using Pycharm2021 (Python) as the programming environment. The input patch size of the MRCNN model was 9×9 , the number of channels was 6, the batch size was 500, the number of iterations was 157, and the number of epochs was 1000. The loss curve and accuracy curve of MRCNN during the training process are shown in Figure 7. The model converged after 1000 epochs.

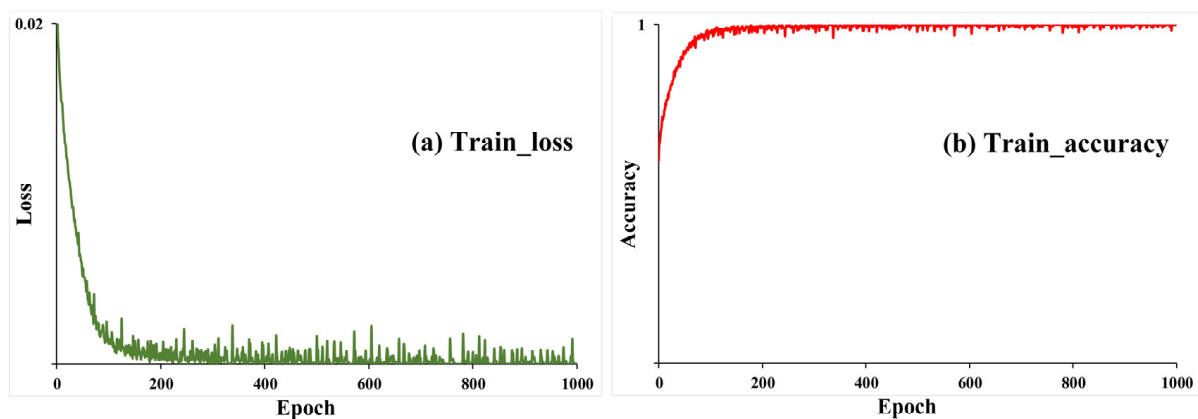


Figure 7. Loss curve and accuracy curve of the training set of MRCNN model.

Table 4 shows that the accuracy and recall reached 99% and 95%, respectively. Although it is not objective to directly compare the two metrics, such high accuracy and recall indicate that the effectiveness of all three algorithms is high. Owing to the substantial difference between the number of samples of *S. alterniflora* and the number of background samples, the precision was relatively low. Even in the period when the distribution area of *S. alterniflora* was the largest in Jiangsu, the percentage of *S. alterniflora* pixels on the satellite images used in this study was only 0.8%. However, the vast majority of *S. alterniflora* samples were identified by the MRCNN according to the recall and accuracy indicators. To reduce the impact of low precision caused by the large number of image pixels and the small proportion of target pixels, this study improved the precision through post-processing.

The results of the post-processing served for the subsequent analysis and discussion of the invasion process of *S. alterniflora*. Meanwhile, the F1-score was used to scientifically and effectively measure the indicators of the algorithms in the binary classification. This study focused on using the F1-score to evaluate the advantages of MRCNN over other comparative algorithms.

Table 4. The extraction results (%) of *S. alterniflora* each year along the coast of Jiangsu.

Period	Method	Accuracy	Recall	Precision	F1-Score
1995	CascadeNet	99.94	99.45	37.57	54.54
	Dual-tunnel CNN	99.95	99.61	38.94	55.99
	MRCNN	99.95	99.68	41.99	59.09
2000	CascadeNet	99.63	97.43	23.58	37.97
	Dual-tunnel CNN	99.75	96.95	31.54	47.59
	MRCNN	99.70	98.35	27.68	43.20
2005	CascadeNet	99.78	98.45	35.31	51.98
	Dual-tunnel CNN	99.69	98.74	28.05	43.69
	MRCNN	99.82	95.97	40.99	57.45
2010	CascadeNet	99.61	97.79	26.84	42.12
	Dual-tunnel CNN	99.60	98.38	26.42	41.65
	MRCNN	99.70	98.44	31.84	48.12
2015	CascadeNet	99.62	97.60	29.11	44.84
	Dual-tunnel CNN	99.42	98.75	21.33	35.08
	MRCNN	99.62	97.42	28.95	44.64
2020	CascadeNet	99.76	97.62	39.83	56.58
	Dual-tunnel CNN	99.64	98.82	31.23	47.46
	MRCNN	99.78	97.94	42.07	58.86

Table 4 shows the classification result of the MRCNN. The F1-score of the MRCNN was the highest in 1995, 2005, 2010, and 2020. In 2000 and 2015, there was only a small gap between the F1-score of the MRCNN and that of the highest model. It is normal for results to vary from year to year owing to differences in imaging conditions. However, in general, the performance of the MRCNN was the best among the three algorithms in most years. After post-processing, the classification precision of *S. alterniflora* was greatly improved, and the annual F1-score was more than 80%, indicating that the combination of the MRCNN and post-processing method was suitable for the identification of *S. alterniflora* in Jiangsu coastal wetland from long time series data. The results of post-processing are shown in Table 5.

Table 5. Classification precision (%) after post-processing.

Period	Method	Precision	F1-Score
1995	MRCNN + Post Processing	70.23	82.40
2000	MRCNN + Post Processing	69.33	81.32
2005	MRCNN + Post Processing	73.67	83.35
2010	MRCNN + Post Processing	68.28	80.63
2015	MRCNN + Post Processing	76.55	85.73
2020	MRCNN + Post Processing	75.68	85.38

Taking 2020 as an example, the identification and comparison of *S. alterniflora* in several typical local areas are shown in Figure 8. For each group, the left image is the combination of the NIR-R-G bands, the middle image is the classified comparison map, and the right image is the ground truth map. All three models can identify the *S. alterniflora* samples well, and the contours of the *S. alterniflora* patches are also relatively consistent. However, the MRCNN model was more accurate, especially in reducing misclassified pixels. On the

premise of ensuring the accuracy, the MRCNN method combined with post-processing proposed in this study greatly reduced the number of misclassified pixels, which met the requirements for *S. alterniflora* identification in this study.

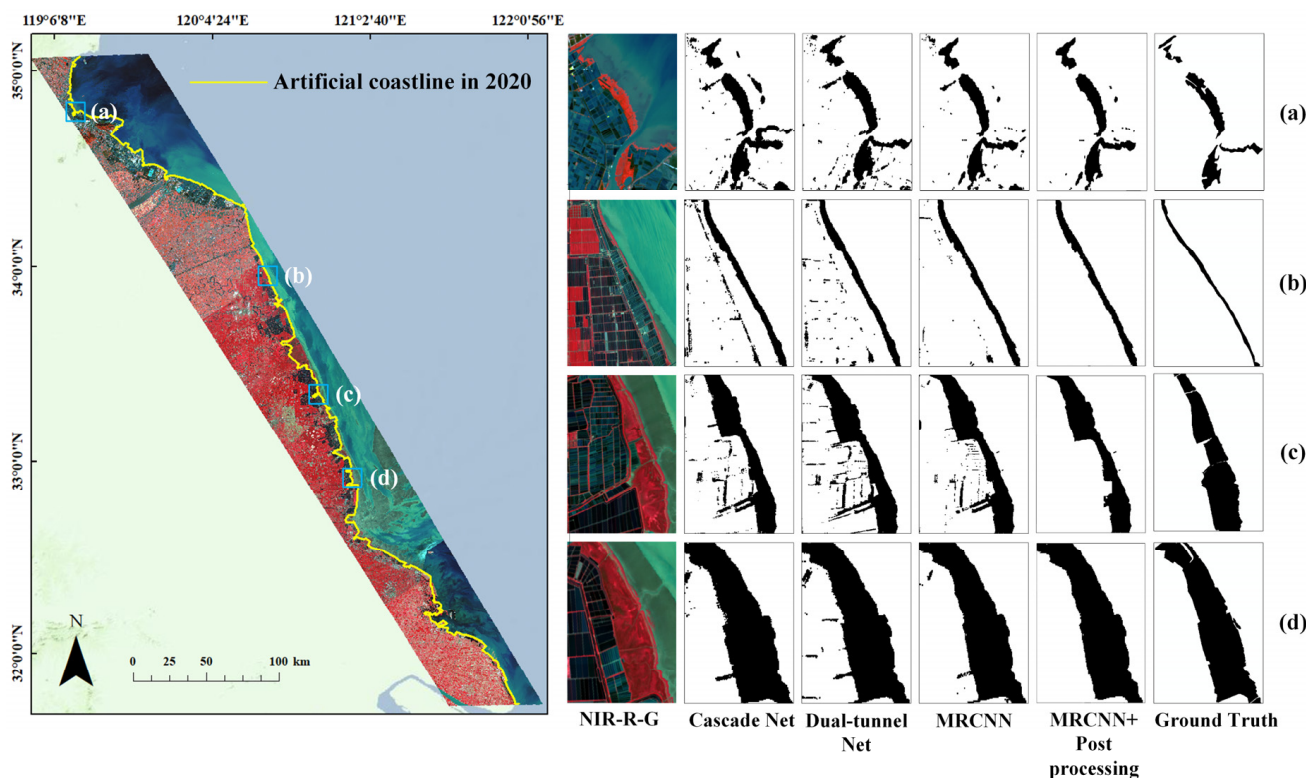


Figure 8. Classification results of *S. alterniflora* in typical regions in 2020. The yellow line is the artificial coastline of Jiangsu in 2020. (a) Linhong River Estuary. (b) Slender strip of *S. alterniflora* north of Sheyang River Estuary. (c) South of RCCNNR. (d) North of Dafeng Port Development Zone.

4.2. Temporal and Spatial Distribution of *S. alterniflora*

4.2.1. Classification of *S. alterniflora*

The experiments showed that the MRCNN model was able to identify *S. alterniflora* in long time series data. In this study, the classification results of *S. alterniflora* in the coastal wetlands of Jiangsu Province were obtained through the MRCNN plus post-processing method and Landsat data from 1990 to 2020. Before determining the area of *S. alterniflora*, it was necessary to manually correct the misclassified and missed classification pixels. After morphological processing, the thematic map of *S. alterniflora* distribution was finally created (as shown in Figure 9). This allowed better analysis of changes in the temporal and spatial distribution of *S. alterniflora*.

In 1990, *S. alterniflora* was first detected at the estuaries of the Linhong River, Guan River, Guboshanghou River, Sheyang River, and Dongtai River. Small patches of *S. alterniflora* also appeared in the south of the RCCNNR, while there was no sign of *S. alterniflora* invasion in the ENNR. In 1995, the north–south length of the *S. alterniflora* patch south of the Sheyang estuary was 6.2 km, while the length of the *S. alterniflora* strip in Lianxinggang reached 19.9 km. By 2000, the coastal areas of the RCCNNR and ENNR had been surrounded by *S. alterniflora* strips, and the nature reserves protected *S. alterniflora* as well as protecting indigenous species. *S. alterniflora* strips were distributed from the Sheyang River estuary to the south of the Dongtai River estuary, spanning 111.5 km from north to south, and *S. alterniflora* strips approximately 12.4 km long had formed near the Linhong River estuary. In 2005, the distribution of *S. alterniflora* in Yancheng City tended to be saturated. From 2010 to 2020, the strips of *S. alterniflora* were substantially damaged, especially in the Dafeng port area.

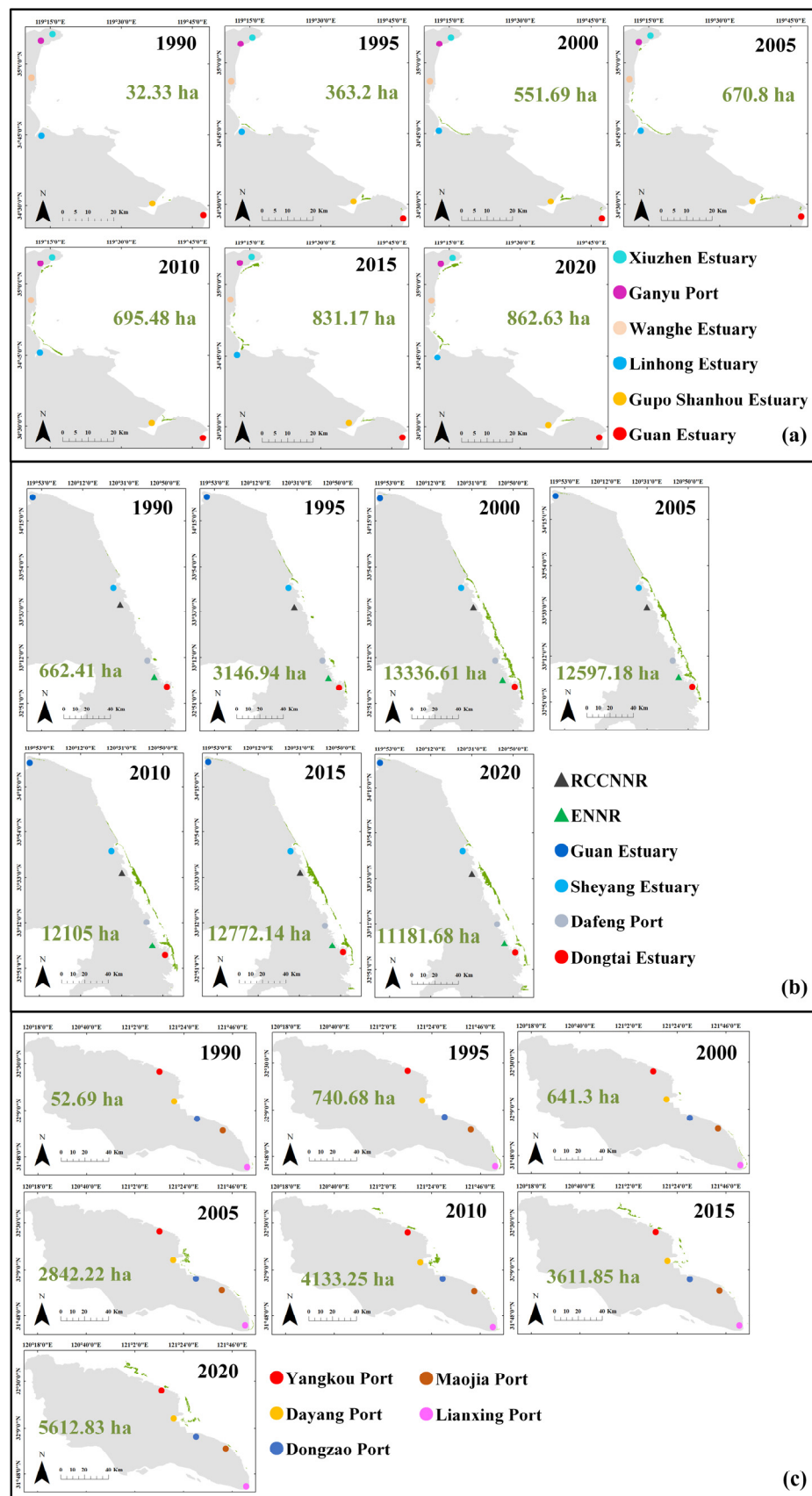


Figure 9. Distribution area (ha) of *S. alterniflora* in coastal wetlands of Jiangsu province from 1990 to 2020. Green is *S. alterniflora*. (a) Lianyungan; (b) Yancheng; (c) Nantong.

4.2.2. Temporal Changes in *S. alterniflora*

The distribution statistics of *S. alterniflora* in Jiangsu Province are shown in Figure 10. In the current study, the expansion of *S. alterniflora* was divided into three stages: the growth stage, outbreak stage, and plateau stage. *S. alterniflora* was in the growth stage before 1995. From 1996 to 2005, it entered the outbreak stage, with a rapid growth rate of 1186 ha/year, mainly distributed in Yancheng. After 2005, it gradually entered the plateau stage. By 2020, the distribution area of *S. alterniflora* in Jiangsu Province had reached 17657.14 ha, an increase of nearly 23.6 times compared with 1990. The changing trend in *S. alterniflora* in the three coastal cities was roughly consistent with the general trend in Jiangsu Province. *S. alterniflora* was first introduced in Yancheng (marked in red in Figure 10). After several rounds of trial planting from 1982 to 1986, *S. alterniflora* entered the outbreak stage earlier in Yancheng than elsewhere. From 1990 to 1995, the expansion rate had reached 496.9 ha/year.

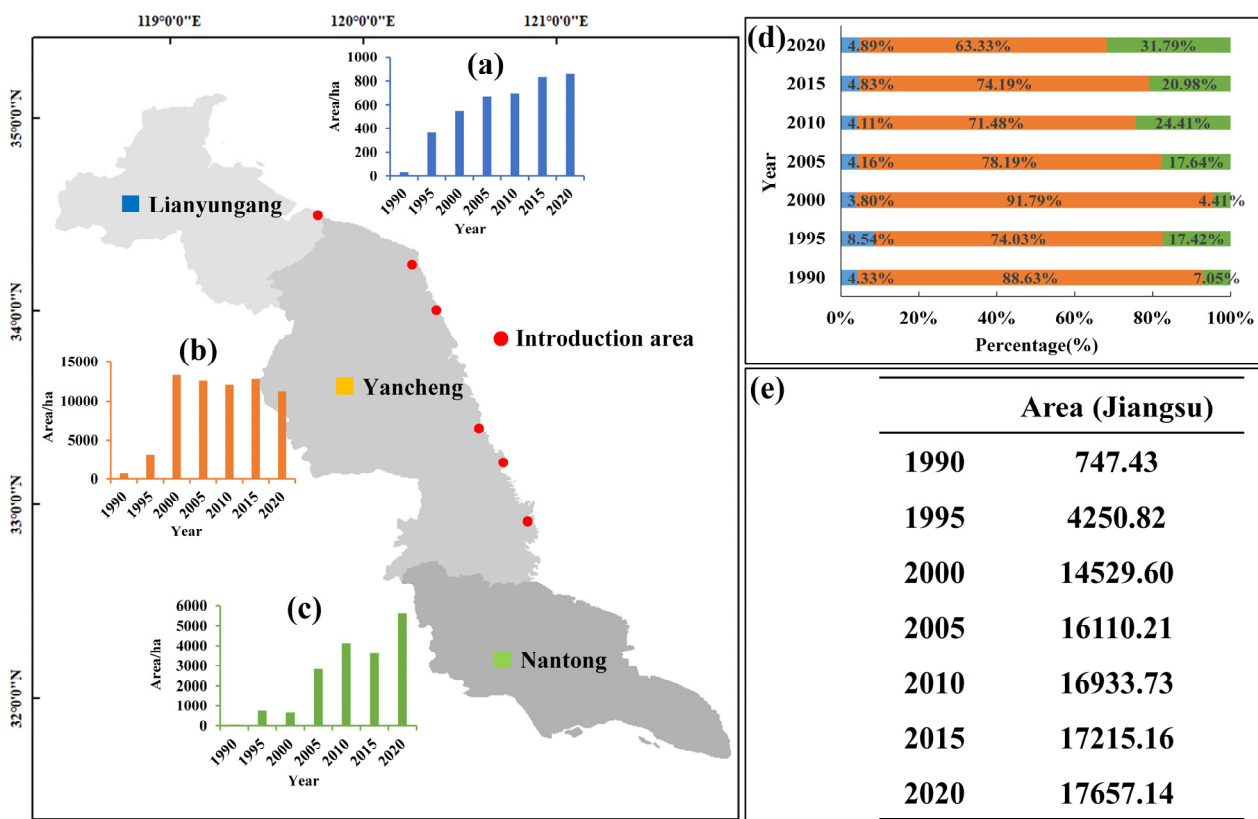


Figure 10. Statistical data of *S. alterniflora* area (ha) in Jiangsu Province from 1990 to 2020. The red mark is the introduction zone of *S. alterniflora* in Yancheng. (a–c) Statistics on the area of *S. alterniflora* in three coastal cities. (d) The distribution proportion (%) of *S. alterniflora* in three coastal cities from 1990 to 2020. (e) Statistical table of the area of *S. alterniflora* in Jiangsu Province.

4.2.3. Spatial Changes in *S. alterniflora*

S. alterniflora patches were defined in this study with a 2-pixel gap (60 m) (Figure 11h). There were two kinds of spatial variation of the centroid of *S. alterniflora* patches. The first one was an expansion parallel to the coastline, which covered the whole range of muddy tidal flats in Jiangsu. The second one was expansion in the direction perpendicular to the coastline, with a relatively small expansion range; the farthest distance to the sea is approximately 4 km. Figure 11 shows that the centroid of *S. alterniflora* patches in Yancheng from 1990 to 2005 expanded from the south and the north to the middle to saturation. During this period, *S. alterniflora* was in the outbreak period, with active artificial reclamation activities and an obvious increase in the number of broken patches.

From 2005 to 2010, the patch centroid of *S. alterniflora* in the RCCNNR and ENNR expanded to the north and south sides to find new ecological niches. Owing to the strengthening of the management of national nature reserves and the reduction of human interference factors, the broken patches of *S. alterniflora* gradually connected, resulting in a decrease in the number of patches. The number of patches of *S. alterniflora* in Jiangsu Province was the largest in 2005, which also marked the end of the outbreak stage of *S. alterniflora* in Jiangsu Province.

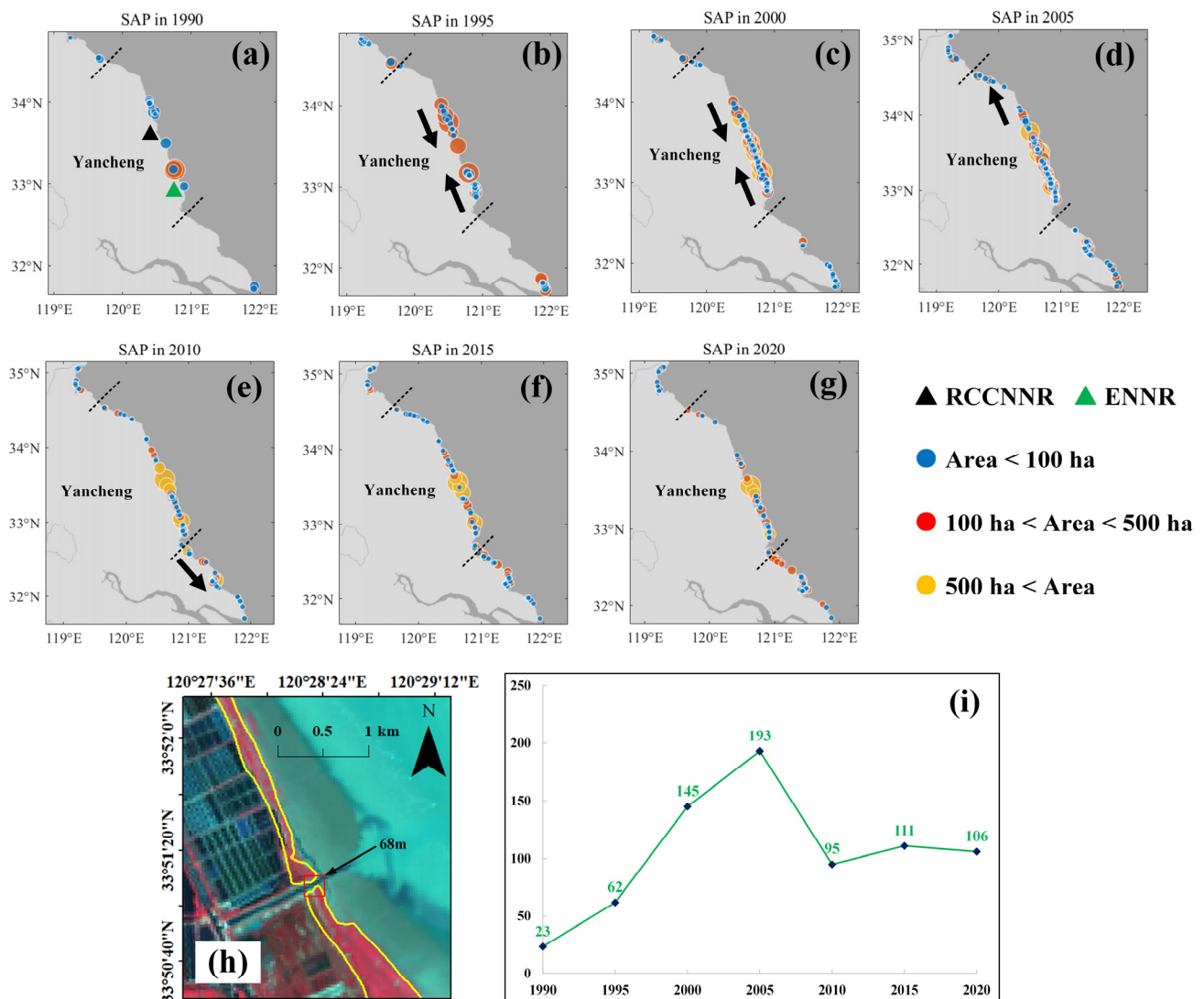


Figure 11. (a–g) Distribution of centroid of *S. alterniflora* patch (SAP) in Jiangsu from 1990 to 2020. There are three levels of patch area. (h) The yellow envelope is the patch boundary of *S. alterniflora*, and the distance between the two patches is 68 m. Combined images of NIR-R-G band. (i) Number of *S. alterniflora* patches in Jiangsu each year.

In Jiangsu Province, the patches of *S. alterniflora* were most densely distributed in Yancheng, and the changes were most obvious. There are two national nature reserves in the area from Dawa Port to the estuary of Dongtai River, where the patch distribution of *S. alterniflora* showed the most obvious changes. The RCCNNR is located between Xinyang Port and Doulong Port. Mudflats were widely distributed in this area, and these were replenished by natural sedimentation. The centroid change of *S. alterniflora* patches from Xinyang Port to Doulong Port from 1995 to 2000 is shown in Figure 12a. The number of *S. alterniflora* patches in the outbreak stage increased significantly, and a large number

of ecological niches were suitable for invasion by *S. alterniflora*. These patches expanded significantly towards the sea, with an average width of 1.1 km. Figure 12b shows the changes in the centroid of *S. alterniflora* patches from Doulong Port to Dafeng Port from 2000 to 2010. Artificial reclamation led to the seaward expansion of *S. alterniflora* patches between Doulong Port and Dafeng Port. The number of *S. alterniflora* patches in this area was clearly reduced, and the expansion distance was relatively small, with an average of 0.8 km to the sea.

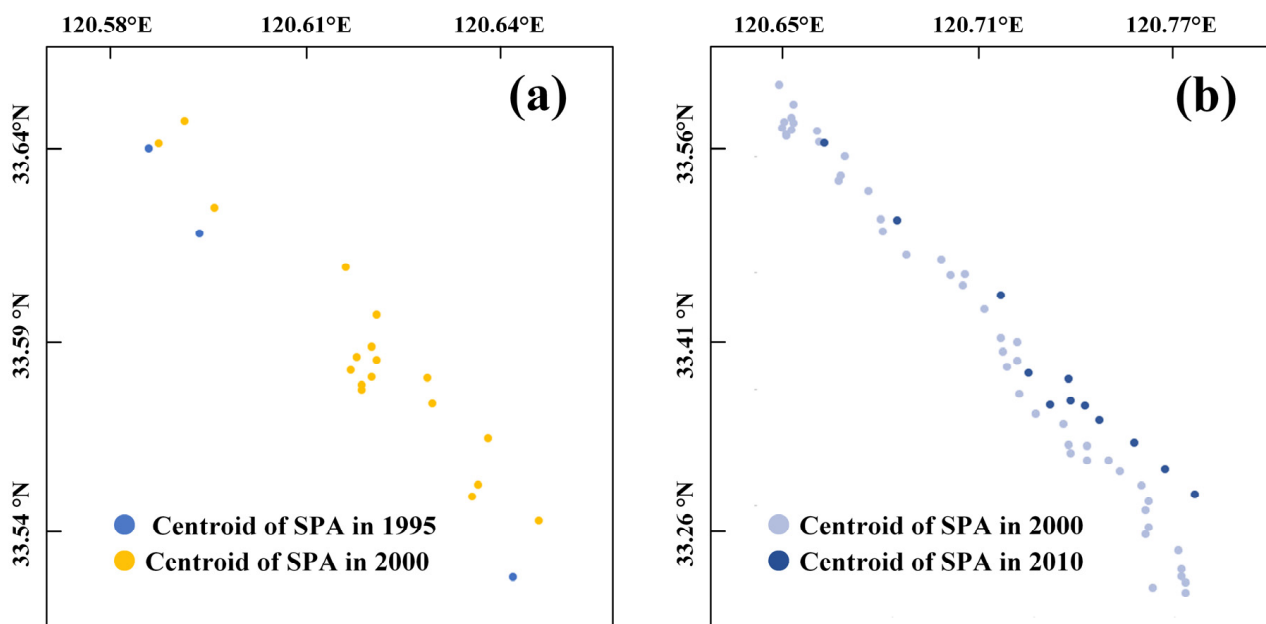


Figure 12. (a) Distribution of centroids of *S. alterniflora* patches (SAP) between Xinyang Port and Doulong Port in 1995 and 2000. (b) Distribution of centroids of *S. alterniflora* patches between Doulong Port and Dafeng Port in 2000 and 2010.

5. Discussion

5.1. The Relationship between Inception Block and Patch Characteristics

The depth and width of the network structure are very important when extracting *S. alterniflora* patches with complex growth states from remote sensing images. The comparison algorithms, CascadeNet, and dual-tunnel CNN, selected in this study mainly used a 3×3 single scale convolutional kernel to extract features. Research [52] showed that using a single convolution kernel can easily lead to filter co-adaptation, resulting in the misclassification of background pixels and target pixels and unclear patch boundaries of *S. alterniflora*. Therefore, the Inception block of the MRCNN network proposed in this study used three convolutional layers with different convolution kernel sizes to extract sample features simultaneously.

After many experiments and comparisons, this study finally selected three convolution kernels: 1×1 , 3×3 , and 5×5 . When the same receptive field is reached, as the convolution kernel decreases, fewer parameters are needed in the training process. As the convolution kernel increases, the number of parameters increases, the complexity of the model increases, and the convergence of the model becomes more difficult. For images with a 30 m spatial resolution, the recognition ranges of 1×1 , 3×3 , and 5×5 convolution kernels are equivalent to $9 \times 10^2 \text{ m}^2$, $2.7 \times 10^3 \text{ m}^2$, and $2.25 \times 10^4 \text{ m}^2$, respectively. These scale capacities were sufficient to accommodate the patch feature information of *S. alterniflora* in various growth states (as shown in Figure 13). The function of the 1×1 convolution layer was mainly to increase the depth of the network, add nonlinear information, and also reduce the dimension and parameters in the training process. For the 3×3 convolution layer, the detailed information of small patches could be better captured, and the ability

to distinguish the boundaries of different objects was enhanced. For the boundaries and mixed zones of *S. alterniflora* patches, a 5×5 convolution layer could obtain smoother features than small-sized convolutional kernels. The multi-scale convolution interaction allowed different strategies to be used to serve the feature information at different scales.

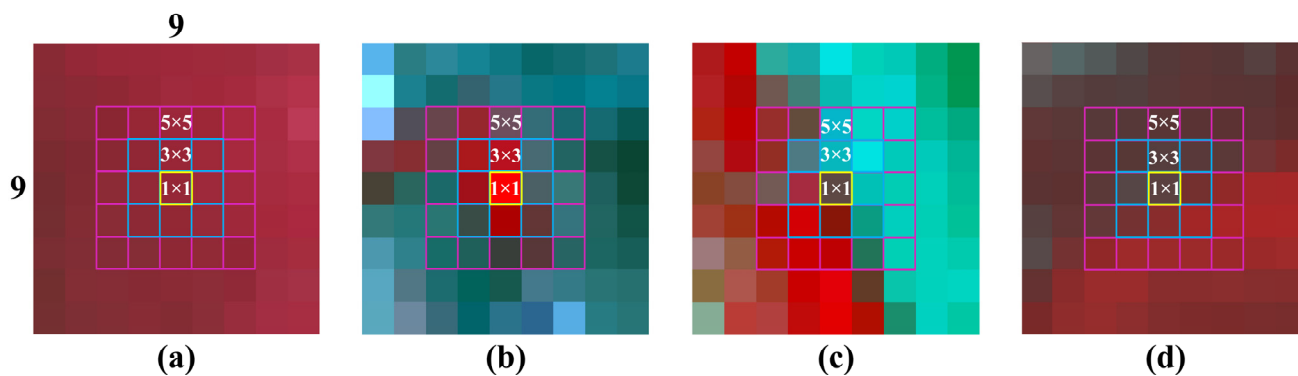


Figure 13. Effects of different receptive fields on the feature extraction of *S. alterniflora*. Combined images of NIR-R-G band. Bright red pixels are *S. alterniflora*. Three different colored grids represent convolution kernels of different sizes. (a) Full coverage of *S. alterniflora*. (b) Small patch of *S. alterniflora*. (c) The boundary between *S. alterniflora* patch and tidal flat. (d) Mixed zone of *S. alterniflora* and *Suaeda*.

5.2. Expansion Factors of *S. alterniflora*

According to literature [53,54], the seed yield of *S. alterniflora* and the silting environment of offshore tidal flats are the main factors that affect the expansion of *S. alterniflora*. The germination rate of *S. alterniflora* seeds on the offshore tidal flat and sporadic patches was significantly higher than that inside the large patches. The sedimentation rate of the offshore tidal flat was mainly affected by natural sedimentation and artificial reclamation [55–57]. Artificial reclamation of the tidal flat changed its sedimentary environment. The decrease in tidal sediment carrying capacity led to the acceleration of the sedimentation rate, promoting the expansion of *S. alterniflora* on the offshore tidal flat [58], and eventually connecting the strips with larger spans. At the same time, excessive reclamation destroyed the habitat for *S. alterniflora*, split *S. alterniflora* patches, and reduced seed yield, which hindered the expansion of *S. alterniflora*.

The implementation of artificial reclamation had a great influence on the coastal environment, and the construction of reclamation changed the hydrodynamic conditions and sediment deposition rate in this area [59]. The tidal flat reclamation area located in Haizhou Bay in the north of Jiangsu Province was substantial, resulting in the siltation of the upper reaches of the Linhong estuary. The average velocity of the flood tide and ebb tide in the reclamation area decreased, which led to sediment deposition [44,60,61] and promoted the expansion of *S. alterniflora* patches toward the sea [62]. The width of the *S. alterniflora* patch extending to the sea in the upper reaches increased from 0.13 km in 2010 to 0.59 km in 2015. Figure 14a shows that the area of *S. alterniflora* in the Linhong River estuary was 67.14 ha in 2010 and increased to 281.96 ha after 5 years. After the Sheyang estuary project was built, the sediment concentration at the flood tide was obviously greater than that at the ebb tide. At the flood tide, more sediment was deposited on both sides of the estuary, which facilitated the expansion of *S. alterniflora* patches to the sea and provided a good niche for the growth of *S. alterniflora*. In 2015, the area of *S. alterniflora* in the Sheyang estuary was 356.99 ha. Five years later, the area of *S. alterniflora* increased to 536.35 ha (Figure 14b), with a remarkable growth rate of 35.87 ha/year.

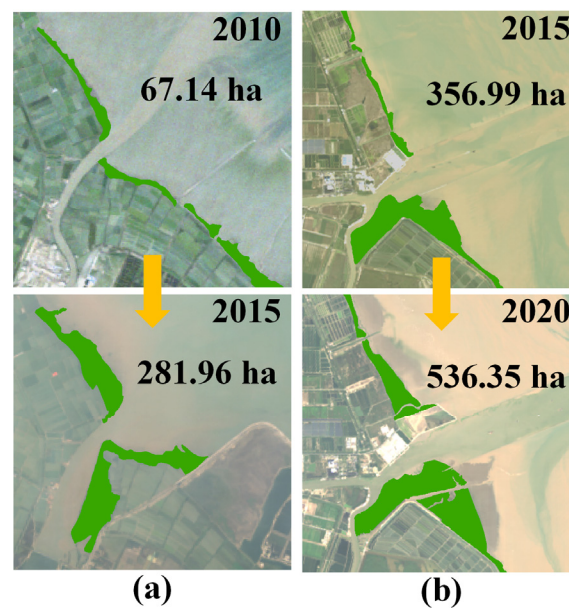


Figure 14. Landsat R-G-B images. Green is *S. alterniflora*. (a) The distribution area of *S. alterniflora* in the estuary of Linhong River from 2010 to 2015. (b) The distribution area of *S. alterniflora* in the estuary of Sheyang River from 2015 to 2020.

Before 2005, *S. alterniflora* was not found in Ganyu Port. After the aquaculture ponds were dismantled in 2000, *S. alterniflora* patches were found in 2005 (Figure 15). The removal of aquaculture ponds is an important habitat modification for the reproduction and growth of *S. alterniflora* seeds. According to research [63,64], the sediment of aquaculture ponds is rich in nitrogen and phosphorus. Owing to the decomposition of excreta from aquaculture species, a large amount of organic nitrogen and phosphorus was released and retained in the sediment, which led to the eutrophication of the aquaculture pond system. With this additional nitrogen, the biomass of *S. alterniflora* grassland increased significantly. The increased nitrogen input stimulated the growth of *S. alterniflora* seeds and improved their productivity [42]. In the past 20 years, *S. alterniflora* in Ganyu Port has increased by nearly 384.71 ha.

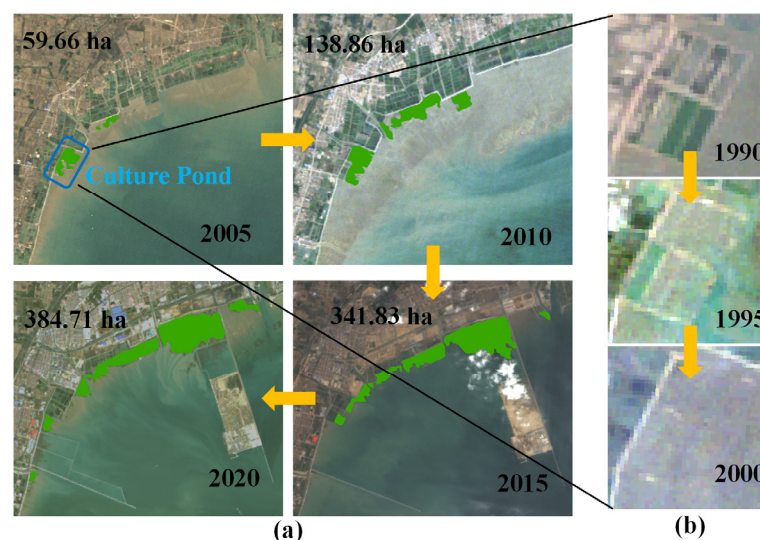


Figure 15. Landsat RGB images. Green is *S. alterniflora*. (a) The distribution area of *S. alterniflora* in Ganyu Port from 2005 to 2020. (b) The demolition process of artificial culture pond (blue rectangular frame) from 1990 to 2000.

In summary, the effect of tidal flat reclamation is closely related to the expansion process of *S. alterniflora*. Reclamation of the tidal flat affects the expansion of *S. alterniflora*, while the growth of *S. alterniflora* patches also leads to a process of stagnation and silting [46]. Sporadic patches were formed by vegetative propagation of *S. alterniflora* in the growth stage, and the planting density gradually increased [3,4]. Subsequently, *S. alterniflora* gradually expanded to the sea through the natural sedimentation and artificial reclamation of tidal flats. In the outbreak stage, the seed yield of *S. alterniflora* increased greatly and drifted along the tidal creeks. Tidal flat reclamation led to a decrease in the hydrodynamic force near the estuary, allowing the seeds to easily take root and grow in the muddy environment and gradually connect into large patches. The ecological niche of *S. alterniflora* was gradually saturated, and finally evolved into a strip pattern with a north–south distribution [62]. *S. alterniflora* is limited by the elevation and tide during the plateau period, and thus it is necessary for the tidal flat on the seaward side to continue silting up before *S. alterniflora* patches can continue to expand seaward.

5.3. Effects of Mixed Pixels and Tidal Inundation on Classification Results

Pixel-level classification algorithms are dependent on the quality of pixels. The influence of cloud cover needs to be considered when selecting image data. In areas covered by clouds, pixel information will be lost. In the initial growth stage of *S. alterniflora*, the proportion of *S. alterniflora* patches in a 30 m pixel was small, and the Landsat images with a medium resolution of 30 m were limited. In fact, the phenomenon of mixed pixels containing other vegetation types or tidal flats is unavoidable. Classifying pixels with mixed vegetation types has always been a challenge in land cover type mapping [65,66]. In the future, the use of high-resolution satellite images or hyperspectral data for fine monitoring can reduce classification errors and improve the accuracy of *S. alterniflora* distribution mapping.

Finally, *S. alterniflora* grows in intertidal areas, which are easily flooded by periodic tides. It is difficult to classify *S. alterniflora* if it is underwater, whether in field surveys or in satellite images. For example, the spectral characteristics and pixel quality of *S. alterniflora* are affected by flooding [67,68]. Optical data are made up of the reflection spectrum of different ground objects and contain rich spectral information, but the quality of pixels is easily affected by clouds, tides, and other factors. Synthetic aperture radar (SAR) reflects the backscattering ability of different ground objects and is not affected by water bodies. It has the ability to penetrate wetland vegetation and has the characteristics of all-day and all-weather data collection, but it lacks spectral information [69]. The different characteristics of optical images and SAR can be used for image fusion [70], which resolves the influence of tides and clouds on pixel quality. These combined data will better serve to identify *S. alterniflora* in coastal wetlands.

6. Conclusions

S. alterniflora has the characteristics of a complex growth environment and different scales of growth. In this study, a multi-temporal sample dataset of *S. alterniflora* in Jiangsu Province was constructed. Through multi-scale feature extraction and depth residual connection, a classification method for *S. alterniflora* based on an MRCNN and post-processing was designed. The classification results for *S. alterniflora* in Jiangsu Province for 6 years were obtained using the unified training method for multi-temporal data. The results showed that the test set of *S. alterniflora* in 1995 had the highest F1-score, which was more than 59%. The performance of the MRCNN was the best among the three algorithms in most years. After post-processing, the global F1-scores of *S. alterniflora* in Jiangsu were all above 80% in each period. This indicates that the proposed method was effective for the identification of *S. alterniflora* using long time series data over a large area. In this study, a thematic map of the distribution of *S. alterniflora* in Jiangsu Province from 1990 to 2020 was created.

After nearly 40 years of expansion, by 2020, the distribution area of *S. alterniflora* in Jiangsu Province had reached 17657.14 ha, mainly in Yancheng. The expansion process of *S. alterniflora* in time was divided into three stages: the growth period (1982–1994), the outbreak period (1995–2004), and the plateau period (2005–2020). The spatial expansion directions of *S. alterniflora* were mainly parallel to the coastline and perpendicular to the coastline. The reclamation of coastal tidal flats in Jiangsu was one of the main factors affecting the invasion of *S. alterniflora*. The tidal flat reclamation provided a new niche and suitable environment for the growth of *S. Alterniflora*, which accelerated the invasion of *S. alterniflora*. The patches of *S. alterniflora* gradually connected into large strips in the north–south direction.

This research provided an effective approach to solving the application of wetland remote sensing using deep learning algorithms. In the future, to better understand the distribution changes of *S. alterniflora* in different regions, we need to construct a large, accurate, and diverse sample library of *S. alterniflora*. By combining optical data with SAR, the quality of the pixels can be improved. Using a powerful deep learning model to accurately and dynamically monitor the distribution changes of *S. alterniflora* can effectively manage and protect the coastal wetland ecosystem.

Author Contributions: W.Z. and G.R. proposed and designed the technique route. W.Z., Z.L., and W.L. contributed to the algorithmic. G.R., N.W., Y.Z. and J.W. (Jianping Wang) were involved in field data collection. W.Z. and Y.H. collected the image data. G.R., S.L. and J.W. (Jianbu Wang) helped with analysis and reviewed the manuscript. All authors have read and agreed to the published version of the manuscript.

Funding: This research was funded by the National Natural Science Foundation of China (Grant No. 42076189 and No. 42106179), the China High-Resolution Earth Observation System Program under Grant 41-Y30F07-9001-20/22, Remote Sensing Monitoring Project of Geographical Elements in Shandong Yellow River Delta National Nature Reserve and Postdoctoral Applied Research Project.

Data Availability Statement: The data are not publicly available due to the confidentiality of the research projects.

Acknowledgments: The author would like to thank the researchers who assisted us in long-term field investigation and data collection.

Conflicts of Interest: The authors declare no conflict of interest.

References

1. Daehler, C.; Strong, D. Hybridization between Introduced Smooth Cordgrass (*Spartina alterniflora*; Poaceae) and Native California Cordgrass (*S. Foliosa*) in San Francisco Bay, California, USA. *Am. J. Bot.* **1997**, *84*, 607. [[CrossRef](#)] [[PubMed](#)]
2. Mao, D.; Liu, M.; Wang, Z.; Li, L.; Man, W.; Jia, M.; Zhang, Y. Rapid Invasion of *Spartina alterniflora* in the Coastal Zone of Mainland China: Spatiotemporal Patterns and Human Prevention. *Sensors* **2019**, *19*, 2308. [[CrossRef](#)] [[PubMed](#)]
3. Ren, G.B.; Wang, J.J.; Wang, A.D.; Wang, J.B.; Zhu, Y.L.; Wu, P.Q.; Ma, Y.; Zhang, J. Monitoring the Invasion of Smooth Cordgrass *Spartina alterniflora* within the Modern Yellow River Delta Using Remote Sensing. *J. Coast. Res.* **2019**, *90*, 135–145. [[CrossRef](#)]
4. Zhang, R.S.; Shen, Y.M.; Lu, L.Y.; Yan, S.G.; Wang, Y.H.; Li, J.L.; Zhang, Z.L. Formation of *Spartina alterniflora* Salt Marshes on the Coast of Jiangsu Province, China. *Ecol. Eng.* **2004**, *23*, 95–105. [[CrossRef](#)]
5. An, S.Q.; Gu, B.H.; Zhou, C.F.; Wang, Z.S.; Deng, Z.F.; Zhi, Y.B.; Li, H.L.; Chen, L.; Yu, D.H.; Liu, Y.H. *Spartina* Invasion in China: Implications for Invasive Species Management and Future Research. *Weed Res.* **2007**, *47*, 183–191. [[CrossRef](#)]
6. Li, B.; Liao, C.; Zhang, X.; Chen, H.; Wang, Q.; Chen, Z.; Gan, X.; Wu, J.; Zhao, B.; Ma, Z.; et al. *Spartina alterniflora* Invasions in the Yangtze River Estuary, China: An Overview of Current Status and Ecosystem Effects. *Ecol. Eng.* **2009**, *35*, 511–520. [[CrossRef](#)]
7. Anttila, C.K.; Daehler, C.C.; Rank, N.E.; Strong, D.R. Greater Male Fitness of a Rare Invader (*Spartina alterniflora*, Poaceae) Threatens a Common Native (*Spartina Foliosa*) with Hybridization. *Am. J. Bot.* **1998**, *85*, 1597–1601. [[CrossRef](#)]
8. Shen, Y.M.; Feng, N.H.; Zhou, Q.; Liu, Y.M.; Chen, Z.Y. The status and its influence of reclamation on Jiangsu coast. *Mar. Sci.* **2006**, *30*, 39–43.
9. Zhu, X.; Meng, L.; Zhang, Y.; Weng, Q.; Morris, J. Tidal and Meteorological Influences on the Growth of Invasive *Spartina alterniflora*: Evidence from UAV Remote Sensing. *Remote Sens.* **2019**, *11*, 1208. [[CrossRef](#)]
10. Deng, Z.; An, S.; Zhou, C.; Wang, Z.; Zhi, Y.; Wang, Y.; Shi, S.; Chen, L.; Zhao, C. Genetic Structure and Habitat Selection of the Tall Form *Spartina alterniflora* Loisel. in China. *Hydrobiologia* **2007**, *583*, 195–204. [[CrossRef](#)]

11. Lu, J.; Zhang, Y. Spatial Distribution of an Invasive Plant *Spartina alterniflora* and Its Potential as Biofuels in China. *Ecol. Eng.* **2013**, *52*, 175–181. [[CrossRef](#)]
12. O'Donnell, J.; Schalles, J. Examination of Abiotic Drivers and Their Influence on *Spartina alterniflora* Biomass over a Twenty-Eight Year Period Using Landsat 5 TM Satellite Imagery of the Central Georgia Coast. *Remote Sens.* **2016**, *8*, 477. [[CrossRef](#)]
13. Bradley, B.A. Remote Detection of Invasive Plants: A Review of Spectral, Textural and Phenological Approaches. *Biol. Invasions* **2014**, *16*, 1411–1425. [[CrossRef](#)]
14. Zuo, P.; Zhao, S.; Liu, C.; Wang, C.; Liang, Y. Distribution of *Spartina* Spp. along China's Coast. *Ecol. Eng.* **2012**, *40*, 160–166. [[CrossRef](#)]
15. Roy, D.P.; Wulder, M.A.; Loveland, T.R.; Woodcock, C.E.; Allen, R.G.; Anderson, M.C.; Helder, D.; Irons, J.R.; Johnson, D.M.; Kennedy, R.; et al. Landsat-8: Science and Product Vision for Terrestrial Global Change Research. *Remote Sens. Environ.* **2014**, *145*, 154–172. [[CrossRef](#)]
16. Mahdianpari, M.; Salehi, B.; Mohammadimanesh, F.; Brisco, B.; Mandavi, S.; Amani, M.; Granger, J.E. Fisher Linear Discriminant Analysis of Coherency Matrix for Wetland Classification Using Po1SAR Imagery. *Remote Sens. Environ.* **2018**, *206*, 300–317. [[CrossRef](#)]
17. Ren, G.B.; Liu, Y.F.; Ma, Y.; Zhang, J. *Spartina alterniflora* Monitoring and Change Analysis in Yellow River Delta by Remote Sensing Technology. *Acta Laser Biol. Sin.* **2014**, *23*, 596.
18. Wang, A.; Chen, J.; Jing, C.; Ye, G.; Wu, J.; Huang, Z.; Zhou, C. Monitoring the Invasion of *Spartina alterniflora* from 1993 to 2014 with Landsat TM and SPOT 6 Satellite Data in Yueqing Bay, China. *PLoS ONE* **2015**, *10*, e0135538. [[CrossRef](#)]
19. Ai, J.; Gao, W.; Gao, Z.; Shi, R.; Zhang, C.; Liu, C. Integrating Pan-Sharpener and Classifier Ensemble Techniques to Map an Invasive Plant (*Spartina alterniflora*) in an Estuarine Wetland Using Landsat 8 Imagery. *J. Appl. Remote Sens.* **2016**, *10*, 026001. [[CrossRef](#)]
20. Sun, C.; Liu, Y.; Zhao, S.; Li, H.; Sun, J. Saltmarshes Response to Human Activities on a Prograding Coast Revealed by a Dual-Scale Time-Series Strategy. *Estuaries Coasts* **2017**, *40*, 522–539. [[CrossRef](#)]
21. Yang, J.F.; Ma, Y.; Ren, G.B.; Zhang, J.Y.; Fan, Y.G. Monitoring method of invasive vegetation *Spartina alterniflora* in modern Yellow River delta based on gf remote sensing data. *Mar. Environ. Sci.* **2017**, *36*, 596–602.
22. Hinton, G.E.; Osindero, S.; Teh, Y.W. A Fast Learning Algorithm for Deep Belief Nets. *Neural Comput.* **2006**, *18*, 1527–1554. [[CrossRef](#)] [[PubMed](#)]
23. Scott, G.J.; England, M.R.; Starns, W.A.; Marcum, R.A.; Davis, C.H. Training Deep Convolutional Neural Networks for Land-Cover Classification of High-Resolution Imagery. *IEEE Geosci. Remote Sens. Lett.* **2017**, *14*, 549–553. [[CrossRef](#)]
24. Zhao, W.; Du, S.; Emery, W.J. Object-Based Convolutional Neural Network for High-Resolution Imagery Classification. *IEEE J. Sel. Top. Appl. Earth Obs. Remote Sens.* **2017**, *10*, 3386–3396. [[CrossRef](#)]
25. Rezaee, M.; Mahdianpari, M.; Zhang, Y.; Salehi, B. Deep Convolutional Neural Network for Complex Wetland Classification Using Optical Remote Sensing Imagery. *IEEE J. Sel. Top. Appl. Earth Observ. Remote Sens.* **2018**, *11*, 3030–3039. [[CrossRef](#)]
26. Rawat, W.; Wang, Z. Deep Convolutional Neural Networks for Image Classification: A Comprehensive Review. *Neural Comput.* **2017**, *29*, 2352–2449. [[CrossRef](#)]
27. Zhong, P.; Wang, R.S. Learning Conditional Random Fields for Classification of Hyperspectral Images. *IEEE Trans. Image Process.* **2010**, *19*, 1890–1907. [[CrossRef](#)]
28. Marmanis, D.; Schindler, K.; Wegner, J.D.; Galliani, S.; Datcu, M.; Stilla, U. Classification with an Edge: Improving Semantic Image Segmentation with Boundary Detection. *ISPRS J. Photogramm. Remote Sens.* **2018**, *135*, 158–172. [[CrossRef](#)]
29. Chen, X.Y.; Xiang, S.M.; Liu, C.L.; Hong, C. Pan Vehicle Detection in Satellite Images by Hybrid Deep Convolutional Neural Networks. *IEEE Geosci. Remote Sens. Lett.* **2014**, *11*, 1797–1801. [[CrossRef](#)]
30. Guo, M.; Yu, Z.; Xu, Y.; Huang, Y.; Li, C. ME-Net: A Deep Convolutional Neural Network for Extracting Mangrove Using Sentinel-2A Data. *Remote Sens.* **2021**, *13*, 1292. [[CrossRef](#)]
31. Hosseiny, B.; Mahdianpari, M.; Brisco, B.; Mohammadimanesh, F.; Salehi, B. WetNet: A Spatial-Temporal Ensemble Deep Learning Model for Wetland Classification Using Sentinel-1 and Sentinel-2. *IEEE Trans. Geosci. Remote Sens.* **2022**, *60*, 4406014. [[CrossRef](#)]
32. Mohammadimanesh, F.; Salehi, B.; Mahdianpari, M.; Gill, E.; Molinier, M. A New Fully Convolutional Neural Network for Semantic Segmentation of Polarimetric SAR Imagery in Complex Land Cover Ecosystem. *ISPRS J. Photogramm. Remote Sens.* **2019**, *151*, 223–236. [[CrossRef](#)]
33. Li, H.; Wang, C.; Cui, Y.; Hodgson, M. Mapping Salt Marsh along Coastal South Carolina Using U-Net. *ISPRS-J. Photogramm. Remote Sens.* **2021**, *179*, 121–132. [[CrossRef](#)]
34. Chen, M.; Ke, Y.; Bai, J.; Li, P.; Lyu, M.; Gong, Z.; Zhou, D. Monitoring Early Stage Invasion of Exotic *Spartina alterniflora* Using Deep-Learning Super-Resolution Techniques Based on Multisource High-Resolution Satellite Imagery: A Case Study in the Yellow River Delta, China. *Int. J. Appl. Earth Obs. Geoinf.* **2020**, *92*, 102180. [[CrossRef](#)]
35. Tian, J.; Wang, L.; Yin, D.; Li, X.; Diao, C.; Gong, H.; Shi, C.; Menenti, M.; Ge, Y.; Nie, S.; et al. Development of Spectral-Phenological Features for Deep Learning to Understand *Spartina alterniflora* Invasion. *Remote Sens. Environ.* **2020**, *242*, 111745. [[CrossRef](#)]

36. Xiong, Z.; Yuan, Y.; Wang, Q. AI-NET: Attention Inception Neural Networks for Hyperspectral Image Classification. In Proceedings of the IGARSS 2018—2018 IEEE International Geoscience and Remote Sensing Symposium, Valencia, Spain, 22–27 July 2018; pp. 2647–2650.
37. Li, H.C.; Hu, W.S.; Li, W.; Li, J.; Du, Q.; Plaza, A. A³ CLNN: Spatial, Spectral and Multiscale Attention ConvLSTM Neural Network for Multisource Remote Sensing Data Classification. *IEEE Trans. Neural Netw. Learn. Syst.* **2022**, *33*, 747–761. [[CrossRef](#)]
38. Zhu, H.; Ma, M.; Ma, W.; Jiao, L.; Hong, S.; Shen, J.; Hou, B. A Spatial-Channel Progressive Fusion ResNet for Remote Sensing Classification. *Inf. Fusion* **2021**, *70*, 72–87. [[CrossRef](#)]
39. Li, G.; Li, L.; Zhu, H.; Liu, X.; Jiao, L. Adaptive Multiscale Deep Fusion Residual Network for Remote Sensing Image Classification. *IEEE Trans. Geosci. Remote Sens.* **2019**, *57*, 8506–8521. [[CrossRef](#)]
40. Alotaibi, B.; Alotaibi, M. A Hybrid Deep ResNet and Inception Model for Hyperspectral Image Classification. *PFG* **2020**, *88*, 463–476. [[CrossRef](#)]
41. Wang, C.; Wang, G.; Dai, L.; Liu, H.; Li, Y.; Zhou, Y.; Chen, H.; Dong, B.; Lv, S.; Zhao, Y. Diverse Usage of Waterbird Habitats and Spatial Management in Yancheng Coastal Wetlands. *Ecol. Indic.* **2020**, *117*, 106583. [[CrossRef](#)]
42. Shen, Y.M.; Zeng, H.; Wang, H.; Liu, Y.M.; Chen, Z.Y. Characteristics of halophyte and associated soil along aggradational muddy coasts in Jiangsu Province. *Acta Ecol. Sin.* **2005**, *25*, 1–6.
43. Shen, Y.M.; Liu, Y.M.; Chen, Q.Z. Analysis of the expanding process of the *Spartina alterniflora* Loisel salt marsh on Jiangsu Province coast by remote sensing. *J. Plant Resour. Environ.* **2002**, *11*, 33–38.
44. Du, J.; Shi, B.; Li, J.; Wang, Y.P. Muddy Coast Off Jiangsu, China: Physical, Ecological, and Anthropogenic Processes. In *Sediment Dynamics of Chinese Muddy Coasts and Estuaries*; Elsevier: Amsterdam, The Netherlands, 2019; pp. 25–49.
45. Ke, C.Q.; Zhang, D.; Wang, F.Q.; Chen, S.X.; Schmullius, C.; Boerner, W.M.; Wang, H. Analyzing Coastal Wetland Change in the Yancheng National Nature Reserve, China. *Reg. Environ. Chang.* **2011**, *11*, 161–173. [[CrossRef](#)]
46. Liu, C.Y.; Zhang, S.Q.; Jiang, H.X.; Wang, H. Spatiotemporal dynamics and landscape pattern of alien species *Spartina alterniflora* in Yancheng coastal wetlands of Jiangsu Province, China. *Ying yong sheng tai xue bao = J. Appl. Ecol.* **2009**, *20*, 901–908.
47. Ouyang, Z.T.; Gao, Y.; Xie, X.; Guo, H.Q.; Zhang, T.T.; Zhao, B. Spectral Discrimination of the Invasive Plant *Spartina alterniflora* at Multiple Phenological Stages in a Saltmarsh Wetland. *PLoS ONE* **2013**, *8*, e67315. [[CrossRef](#)]
48. Gao, Z.G.; Zhang, L.Q. Multi-Seasonal Spectral Characteristics Analysis of Coastal Salt Marsh Vegetation in Shanghai, China. *Estuar. Coast. Shelf Sci.* **2006**, *69*, 217–224. [[CrossRef](#)]
49. Thakkar, V.; Tewary, S.; Chakraborty, C. Batch Normalization in Convolutional Neural Networks—A Comparative Study with CIFAR-10 Data. In Proceedings of the 2018 Fifth International Conference on Emerging Applications of Information Technology (EAIT), Kolkata, India, 12–13 January 2018; pp. 1–5.
50. Li, X.; Li, W.; Xu, X.; Du, Q. CascadeNet: Modified ResNet with Cascade Blocks. In Proceedings of the 2018 24th International Conference on Pattern Recognition (ICPR), Beijing, China, 20–24 August 2018; pp. 483–488.
51. Xu, X.; Li, W.; Ran, Q.; Du, Q.; Gao, L.; Zhang, B. Multisource Remote Sensing Data Classification Based on Convolutional Neural Network. *Ieee Trans. Geosci. Remote Sens.* **2018**, *56*, 937–949. [[CrossRef](#)]
52. Liao, Z.; Carneiro, G. Competitive Multi-Scale Convolution. *arXiv* **2015**, arXiv:1511.05635.
53. Xu, W.W.; Wang, G.X.; Liu, J.E.; Chen, Z.Y.; Wang, G. Seed characteristics and seedling growth of *Spartina alterniflora* on coastal wetland of North Jiangsu. *Acta Ecol. Sin.* **2011**, *31*, 4560–4567.
54. Espinar, J.L.; Thompson, K.; Garcia, L.V. Timing of Seed Dispersal Generates a Bimodal Seed Bank Depth Distribution. *Am. J. Bot.* **2005**, *92*, 1759–1763. [[CrossRef](#)]
55. Xu, N.; Gong, P. Significant Coastline Changes in China during 1991–2015 Tracked by Landsat Data. *Sci. Bull.* **2018**, *63*, 883–886.
56. Bao, J.; Gao, S.; Ge, J. Dynamic Land Use and Its Policy in Response to Environmental and Social-Economic Changes in China: A Case Study of the Jiangsu Coast (1750–2015). *Land Use Policy* **2019**, *82*, 169–180. [[CrossRef](#)]
57. Duan, Y.; Li, X.; Zhang, L.; Liu, W.; Liu, S.; Chen, D.; Ji, H. Detecting Spatiotemporal Changes of Large-Scale Aquaculture Ponds Regions over 1988–2018 in Jiangsu Province, China Using Google Earth Engine. *Ocean. Coast. Manag.* **2020**, *188*, 105144. [[CrossRef](#)]
58. Wang, Y.P.; Gao, S.; Jia, J.; Thompson, C.E.L.; Gao, J.; Yang, Y. Sediment Transport over an Accretional Intertidal Flat with Influences of Reclamation, Jiangsu Coast, China. *Mar. Geol.* **2012**, *291–294*, 147–161.
59. Li, L.; Ye, T.; Wang, X.H.; He, Z.; Shao, M. Changes in the Hydrodynamics of Hangzhou Bay Due to Land Reclamation in the Past 60 Years. In *Sediment Dynamics of Chinese Muddy Coasts and Estuaries*; Elsevier: Amsterdam, The Netherlands, 2019; pp. 77–93.
60. Feng, L.; Zhu, X.; Sun, X. Assessing Coastal Reclamation Suitability Based on a Fuzzy-AHP Comprehensive Evaluation Framework: A Case Study of Lianyungang, China. *Mar. Pollut. Bull.* **2014**, *89*, 102–111. [[CrossRef](#)]
61. Wu, X.W.; Wang, A.J. Impacts of Human Beings' Activities on North Jiangsu Tidal Flat. *Sci. Geogr. Sin.* **2005**, *25*, 614–620.
62. Deng, Z.F.; An, S.Q.; Zhi, Y.B.; Zhou, C.F.; Chen, L.; Zhao, C.J.; Fang, S.B.; Li, H.L. Preliminary studies on invasive model and outbreak mechanism of exotic species, *Spartina alterniflora* Loisel. *Acta Ecol. Sin.* **2006**, *26*, 2678–2686.
63. Mook, W.T.; Chakrabarti, M.H.; Aroua, M.K.; Khan, G.M.A.; Ali, B.S.; Islam, M.S.; Abu Hassan, M.A. Removal of Total Ammonia Nitrogen (TAN), Nitrate and Total Organic Carbon (TOC) from Aquaculture Wastewater Using Electrochemical Technology: A Review. *Desalination* **2012**, *285*, 1–13. [[CrossRef](#)]
64. Jasmin, M.Y.; Syukri, F.; Kamarudin, M.S.; Karim, M. Potential of Bioremediation in Treating Aquaculture Sludge: Review Article. *Aquaculture* **2020**, *519*, 734905.

65. Zhang, X.; Xiao, X.; Wang, X.; Xu, X.; Chen, B.; Wang, J.; Ma, J.; Zhao, B.; Li, B. Quantifying Expansion and Removal of *Spartina alterniflora* on Chongming Island, China, Using Time Series Landsat Images during 1995–2018. *Remote Sens. Environ.* **2020**, *247*, 111916.
66. Wang, J.; Xiao, X.; Qin, Y.; Dong, J.; Geissler, G.; Zhang, G.; Cejda, N.; Alikhani, B.; Doughty, R.B. Mapping the Dynamics of Eastern Redcedar Encroachment into Grasslands during 1984–2010 through PALSAR and Time Series Landsat Images. *Remote Sens. Environ.* **2017**, *190*, 233–246. [[CrossRef](#)]
67. Rogers, K.; Lymburner, L.; Salum, R.; Brooke, B.P.; Woodroffe, C.D. Mapping of Mangrove Extent and Zonation Using High and Low Tide Composites of Landsat Data. *Hydrobiologia* **2017**, *803*, 49–68. [[CrossRef](#)]
68. Li, S.H.; Ge, Z.M.; Xie, L.N.; Chen, W.; Yuan, L.; Wang, D.Q.; Li, X.Z.; Zhang, L.Q. Ecophysiological Response of Native and Exotic Salt Marsh Vegetation to Waterlogging and Salinity: Implications for the Effects of Sea-Level Rise. *Sci. Rep.* **2018**, *8*, 2441. [[CrossRef](#)] [[PubMed](#)]
69. Zhang, X.; Xu, J.; Chen, Y.; Xu, K.; Wang, D. Coastal Wetland Classification with GF-3 Polarimetric SAR Imagery by Using Object-Oriented Random Forest Algorithm. *Sensors* **2021**, *21*, 3395. [[CrossRef](#)]
70. Adeli, S.; Salehi, B.; Mahdianpari, M.; Quackenbush, L.J.; Brisco, B.; Tamiminia, H.; Shaw, S. Wetland Monitoring Using SAR Data: A Meta-Analysis and Comprehensive Review. *Remote Sens.* **2020**, *12*, 2190. [[CrossRef](#)]